This article has been accepted for publication in a future issue of this journal, but has not been fully edited. Content may change prior to final publication. Citation information: DOI 10.1109/TGRS.2021.3128565, IEEE Transactions on Geoscience and Remote Sensing

Phase unwrapping of coarsely sampled maps using higher-order methods

Bhargav Ghanekar*, Uday K Khankhoje†

***Abstract*—We consider the problem of two dimensional phase unwrapping – that of reconstructing the absolute phase (up to a constant) given a noisy 2π-wrapped phase map as input. In particular, we present an algorithm that excels at unwrapping low resolution phase maps, i.e. maps obtained by coarsely sampling a field of view. Our key observation is that the magnitudes of higher-order differences on phase maps are typically much lower than corresponding first order differences. We develop this insight into formulating "higher order Itoh conditions". Using this, we build an optimization-based framework that leverages higher-order information to estimate the first order derivatives of the unwrapped phase with the aid of appropriate total variation and irrotationality-based regularizers. The first order derivatives are then integrated using a minimum spanning tree approach to produce the unwrapped phase map. We compare the performance on synthetic terrain maps and real world data obtained from interferometric synthetic aperture radar with other contemporary algorithms to demonstrate superior performance on key metrics such as absolute error, feature similarity, and image sharpness for low resolution phase maps.**

I. Introduction

Phase unwrapping is a key technique at the heart of many applications in remote sensing, cell imaging, and magnetic resonance imaging, among other areas [1]. In interferometric synthetic aperture radar (InSAR), two SAR images are interfered to produce an image whose phase contains information about the scene topography [2], [3]; however, since the phase information is wrapped modulo 2π, an unwrapping procedure is required in order to obtain the terrain's topography. Similarly, in the case of cell imaging, the measured phase after wave propagation through a sample is proportional to the optical path delay, which indicates the extent of delay as compared to a clear medium. Again, since the recorded phase values are modulo 2π, a phase unwrapping problem needs to be solved in order to accomplish cell imaging [4], [5].

The field of phase unwrapping is rich in techniques developed over the last several decades [1]. It is beyond the scope of this paper to give a comprehensive review of all such techniques, but it suffices to broadly delineate the main approaches (see [6] for an InSAR related review). An idea at the core of most phase unwrapping techniques is that of continuity of the phase across a scene; this implies a certain minimum sampling rate of the imaged scene. Under these conditions, as formally codified in the "Itoh" condition [7] (more on this in Sec. II-A), the wrapped phase maps can be used to estimate the derivatives of the unwrapped phase, which in turn can be integrated to reveal the unwrapped phase. Of course, the presence of system noise or abrupt changes in the true unwrapped phase can lead to this condition being violated. In such a case, one strategy has focused on efficient path-following methods using ideas of branch cuts [8], [9], or minimum spanning trees [10], [11] for phase unwrapping. Yet another approach has been to formulate the problem in an optimization framework; here the difference between gradients of the estimated unwrapped phase map and that given by the Itoh condition are minimized subject to appropriate regularization conditions [12]–[15]. Another set of methods are statistics based, which can fuse apriori information about the imaged scene. For e.g., the SNAPHU method proposed in [16] uses a statistics based network flow model to obtain the most likely unwrapping result. Another popular method in this category, PUMA, treats the objective function of minimization as first-order Markov random fields and computes phase unwrapping by a sequence of max-flow/min-cut calculations [17]. Finally, machine learning techniques have come up in recent years [18]–[22], offering very promising results in terms of both the speed and accuracy of phase unwrapping, but at the cost of significant computational resources for training and open questions about performance on data which is very different from the training set.

Our work is rooted in the optimization approach and addresses a class of problems previously not addressed explicitly – namely that of phase unwrapping of low resolution images. With the upcoming advent of drone based InSAR systems [23], [24], it will be desirable to have technological solutions for reducing the weight and complexity of on-board hardware, and our work is a step in that direction. Similarly, microscopy related applications such as optical coherence tomography [25] and digital holographic microscopy [26] also stand to benefit with lower resolution imaging hardware amidst a push towards building low cost microscopy solutions [27], [28].

The primary challenge with low resolution images is that the Itoh condition gets violated due to abrupt or large changes in phase across adjacent pixels. However, the corresponding changes in higher order finite-differences are lower, and estimating first order phase gradients from

∗Electrical & Computer Engineering, Rice University, Houston, Texas, USA 77005. E-mail: bg40@rice.edu

†Electrical Engineering, Indian Institute of Technology Madras, Chennai, Tamil Nadu, India 600036. E-mail: uday@ee.iitm.ac.in

This article has been accepted for publication in a future issue of this journal, but has not been fully edited. Content may change prior to final publication. Citation information: DOI 10.1109/TGRS.2021.3128565, IEEE Transactions on Geoscience and Remote Sensing

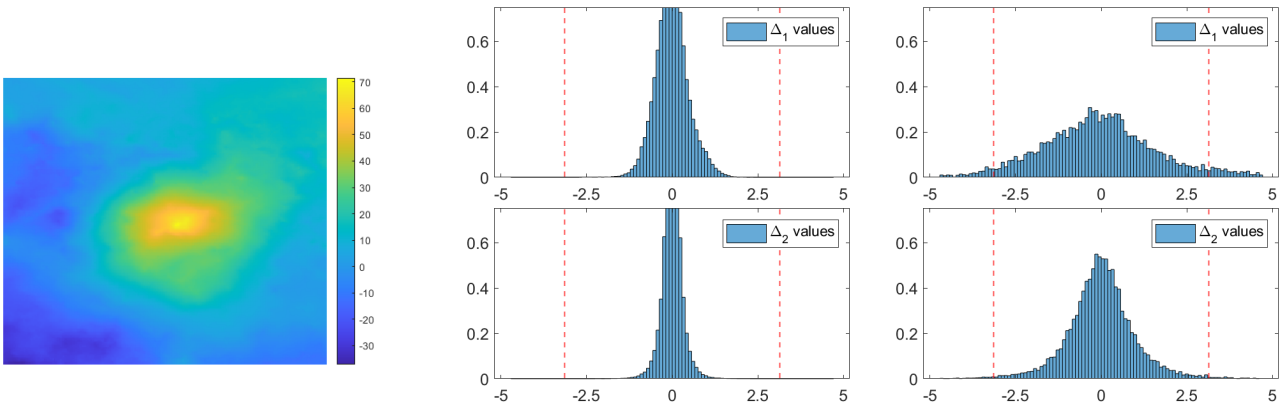

(a) Fine sampled terrain map (b) Histogram – fine map (c) Histogram – coarse map

Fig. 1: (a) A synthetic terrain map and (b,c) normalized histogram plots of first (Δ_1) and second (Δ_2) order gradient magnitudes, respectively, on a simulated terrain map under two sampling cases (fine and coarse). The red vertical lines indicate the limits $\pm\pi$ that are relevant to the Itoh conditions. The histogram width for Δ_2 values is smaller than those for Δ_1 values, especially for the coarsely sampled case – motivating the use of higher order derivatives for unwrapping.

higher order differences opens the door to successfully processing low resolution images (see Fig. 1 for a visual summary of this observation). We formulate higher order Itoh conditions to capture this idea and further regularize the objective function with sparsity based total variation and irrotationality constraints. After identifying problematic points in the reconstruction, we use a minimum spanning tree approach to integrate the obtained phase gradients, thus completing the task of phase unwrapping. We study the working of our algorithm on high and low resolutions images, with different noise levels. We compare our results with techniques that only use first order methods as well as with the popular PUMA algorithm mentioned earlier.

The layout of this paper is as follows. In Section II we describe the higher order Itoh conditions, formulation of the optimization problem, and the integration strategy. In Section III we describe the numerical experiments performed with synthetic and real-world data. Based on these results, we summarize our findings in Section IV. All our computer codes are available here: https://github.com/shadowfax11/phase_unwrap_itvc.

II. Methods

In this Section, we detail some fundamental properties with regards to signal wrapping, and then describe the proposed unwrapping framework.

A. The Itoh condition and its higher order extensions

Given a sequence of N numbers, $\{x_n\}_{n=1}^N$, let its corresponding wrapped sequence $\{w_n\}_{n=1}^N$ be expressed as:

$$w_n = W[x_n] = x_n + 2\pi k_n, \quad k_n \in \mathbb{Z}, \tag{1}$$

such that $w_n \in [-\pi, \pi)$, and $W[.]$ denotes the wrapping operator (modulo 2π operation). Let Δ_1 denote the first order difference operator s.t. $\Delta_1(x_n) = x_n - x_{n-1}$. The Itoh condition [7] relates a sequence to its wrapped version as follows:

$$W[\Delta_1(w_n)] = \Delta_1(x_n) \tag{2}$$

provided the following condition is satisfied:

$$|\Delta_1(x_n)| < \pi, \quad \forall n \tag{3}$$

Thus, one can recover the original sequence $\{x_n\}$ from the wrapped sequence $\{w_n\}$ by a simple summation that uses the Itoh condition:

$$x_k = x_1 + \sum_{i=2}^{k} W[\Delta_1(w_i)], \quad k \in [2, N]. \tag{4}$$

We also show that the Itoh condition can readily be extended to higher order derivatives. We denote an m-th order derivative operator by Δ_m (obtained by a m-th order finite difference operation), and note the following Theorem.

Theorem 1: Given an input sequence of phase values, $\{x_n\}$, a wrapping operator W, and the corresponding wrapped sequence, $\{w_n\}$, then if the m^{th} order difference operator satisfies: $|\Delta_m(x_n)| < \pi$ for all n, the following result holds for $m \geq 1$:

$$W(\Delta_m(W(x_n))) = W(\Delta_m(w_n)) = \Delta_m(x_n) \tag{5}$$

Proof: see Appendix A.

Thus, we state a higher order Itoh condition: Given a wrapped sequence $\{w_n\}$, we can recover $\{\Delta_m x_n\}$ from $w_n = W[x_n]$ if $|\Delta_m(x_n)| < \pi$, and then subsequently integrate to obtain x_n (subject to a priori knowledge on related integration constants). Henceforth, we will refer to the wrapped versions of the derivatives of wrapped phase map as "Itoh estimates"; thus $W[\Delta_1(w_i)]$ is an Itoh estimate, and $W[\Delta_2(w_i)]$ is a second order Itoh estimate. Thus, from Theorem 1, we can infer that for the case of $m = 2$, we can recover the sequence $\{\Delta_1(x_n)\}$ from the wrapped sequence $\{W(\Delta_2(w_n)\}$ using the second-order Itoh estimates as follows:

$$\Delta_1(x_k) = \Delta_1(x_1) + \sum_{i=2}^{k} W[\Delta_2(w_i)], \quad k \in [2, N]. \tag{6}$$

This article has been accepted for publication in a future issue of this journal, but has not been fully edited. Content may change prior to final publication. Citation information: DOI 10.1109/TGRS.2021.3128565, IEEE Transactions on Geoscience and Remote Sensing

and subsequently recover the original sequence $\{x_n\}$ via integration (provided we have information about the absolute phase and gradient value of the initial unwrapping point). Extensions of the higher order Itoh conditions to 2D signals are straightforward and considered in Appendix B.

B. Key difference between fine and coarse maps

This higher order Itoh condition is a more relaxed condition on x_n compared to the first order condition for most phase maps encountered in practice, and is well appreciated by graphic histograms in Fig. 1. Here, histograms of first and second order difference magnitudes on a typical random rough terrain map are displayed. For a finely sampled map, both the first and second order difference magnitudes easily satisfy the respective Itoh conditions.

Whereas, when considering coarsely sampled maps (obtained by downsampling the fine maps by a factor of $4\times$ in each direction), it is evident that the number of points where the first order Itoh condition is violated is much more than the corresponding number the second order condition. Thus, phase unwrapping undertaken with first order derivatives on a coarsely sampled map is likely to be more erroneous than when second order derivatives are considered. This key observation informs the heart of our approach: leverage higher order information for phase unwrapping of coarsely sampled maps.

In fact, we can formally show that the higher order Itoh condition is satisfied more frequently than a lower order Itoh condition for reasonably smooth surfaces, as quantified in the following Theorem.

Theorem 2: Given a sequence of $k-$order derivatives of a surface, $\{g[n]\}$, and the $k+1-$order derivative sequence as $\{h[n]\}$, then the following holds for reasonably smooth surfaces:

$$\text{If } P(|g| > \pi) = C, \text{then } P(|h| > \pi) < C,$$

where P denotes probability.

Proof: See Appendix C.

C. Denoising and irrotationality considerations

The above discussions indicate that the Itoh estimates are *estimates* of the derivatives of the true unwrapped phase map, subject to certain bounds on magnitudes of the derivatives. Thus in principle, we can obtain unwrapped phase derivative estimates from the 1st and 2nd order Itoh estimates, and then integrate them to obtain the true unwrapped phase map. This idea, however, must be tempered by the fact that input wrapped phase maps are noise corrupted. Furthermore, the act of finite differencing amplifies this noise [29]. As a result, the obtained 1st or 2nd order Itoh estimates will be noisier – more so for the 2nd order as compared to the 1st order Itoh estimates.

Therefore it is essential to denoise the obtained derivative estimates prior to integration. A popular approach for denoising is to use total variation methods [30]–[32].

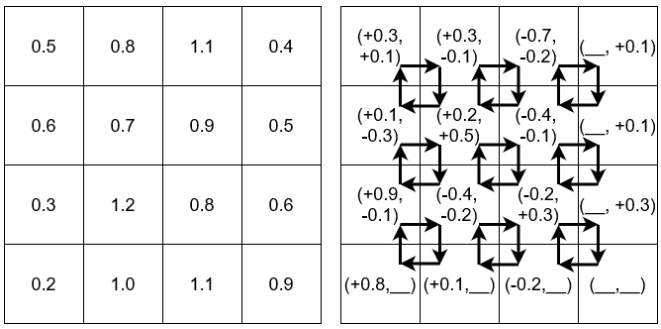

Fig. 2: Left: Phase map values, f (in multiples of 2π), Right: Derivative $(\Delta_x f, \Delta_y f)$ values. Every 2×2 loop summation of gradients map must be zero.

These methods are suitable since they preserve jump discontinuities and suppress the noise induced by numerical differentiation [29]. Indeed, performing 2D unwrapping by denoising 1st order Itoh estimates by total variation denoising has been performed successfully [14], [33]. In our methods, we also adopt total variation methods (and higher-order variants) for the purpose of denoising.

In the case of 2D signals, derivative denoising involves an additional constraint that comes from the irrotationality or integrability property of 2D surfaces [34]: any summation of the gradients across a loop of 2×2 pixels on the map must be zero (See Fig. 2; the guiding principle is this – for a scalar differentiable function $f(x, y)$, whose gradient is given by ∇f, the integral identity $\oint_C \nabla f \cdot d\vec{l} = 0$ holds independent of the path chosen, C). If this condition is not satisfied, the estimates are erroneous and the integration of the x, y-derivative estimates will not be path-independent, both of which are highly undesirable. We use the above observations to *regularize* the derivative estimates in such a way that while they are close to the Itoh estimates, they *also* satisfy the irrotationality property.

D. Optimization problem formulation

We are now in a position to formally outline our novel 2D phase unwrapping algorithm, the *central idea* of which is: Utilize second order Itoh estimates to correctly estimate the first order phase map derivatives $\rightarrow$ the unwrapped phase map estimate is then obtained by integrating the x, y-derivatives over consistent gradients. This is done iteratively over each residual map for a fixed number of times to obtain the final estimated unwrapped phase map.

Given an input wrapped map b, possibly corrupted by noise, we propose the following convex optimization problem to implement the central idea:

$$\begin{aligned}\hat{\mathbf{f}}_x, \hat{\mathbf{f}}_y = \underset{f,g}{\operatorname{argmin}}\ & \epsilon_1 \left\|\mathbf{f} - \mathbf{b}_f\right\|_2^2 + \epsilon_2 \left\|\mathbf{g} - \mathbf{b}_g\right\|_2^2 \\ & + \lambda_1 \mathrm{TV}(\mathbf{f}) + \lambda_2 \mathrm{TV}(\mathbf{g}) \\ & + \beta_1 \left\|M_1 \mathbf{f}\right\|_1^1 + \beta_2 \left\| \begin{bmatrix} M_2 & 0 \\ 0 & M_3 \end{bmatrix} \mathbf{g} \right\|_1^1 \\ & + \mu_1 \left\|\nabla \mathbf{f} - \mathbf{g}\right\|_2^2 + \mu_2 \left\|\mathbf{g}_{xy} - \mathbf{g}_{yx}\right\|_2^2\end{aligned} \tag{7}$$

where:

This article has been accepted for publication in a future issue of this journal, but has not been fully edited. Content may change prior to final publication. Citation information: DOI 10.1109/TGRS.2021.3128565, IEEE Transactions on Geoscience and Remote Sensing

- $\mathbf{f} = \left[\mathbf{f}_x^T, \mathbf{f}_y^T\right]^T$ and $\mathbf{g} = \left[\mathbf{g}_{xx}^T, \mathbf{g}_{xy}^T, \mathbf{g}_{yx}^T, \mathbf{g}_{yy}^T\right]^T$ respectively correspond to concatenated vectors of the vectorized versions of the first and second derivative maps of the unwrapped phase map. Henceforth, all variables indicated in bold correspond to flattened-out column vectors of the corresponding 2D variable (which are expressed in non-boldface font).
- $\mathbf{b}_f, \mathbf{b}_g$ correspond to stacked vectors of 1st and 2nd order 2D Itoh estimates of input b given in Eqns. 16–20 (See Appendix B). Thus, the first two terms, weighted by hyperparameters ϵ_1, ϵ_2, correspond to a "data fit" term in the cost function.
- TV($\mathbf{f}$) corresponds to the sum of the TV norms of $\mathbf{f}_x$, $\mathbf{f}_y$, while TV($\mathbf{g}$) corresponds to the sum of the TV norms of $\mathbf{g}_{xx}$, $\mathbf{g}_{yx}$, $\mathbf{g}_{xy}$, $\mathbf{g}_{yy}$; these terms act to denoise the derivatives and are weighted by hyperparameters λ_1, λ_2, respectively.
- To check for irrotationality of derivative maps (say $\hat{f}_x$ and $\hat{f}_y$), one needs to ensure that at all points (i,j), a 2x2 loop summation equals zero, i.e.

$$\hat{f}_x(i,j) + \hat{f}_y(i,j+1) - \hat{f}_x(i+1,j) - \hat{f}_y(i,j)$$

$$\implies \left[1,-1,1,-1\right] \begin{bmatrix} \hat{f}_x(i,j) \\ \hat{f}_x(i+1,j) \\ \hat{f}_y(i,j+1) \\ \hat{f}_y(i+1,j+1) \end{bmatrix} = 0$$

  Such constraint equations can be written together in a matrix format. Thus, M_1, M_2, M_3 are sparse matrices, with each row in the matrices having only 4 non-zero elements (from the set $\{+1,-1\}$), corresponding to a 2×2 loop summation at a point. Specifically, M_1, M_2, M_3 correspond to the irrotationality operator when used upon the stacked vectors $\left[\mathbf{f}_x^T, \mathbf{f}_y^T\right]^T$, $\left[\mathbf{g}_{xx}^T, \mathbf{g}_{xy}^T\right]^T$, $\left[\mathbf{g}_{yx}^T, \mathbf{g}_{yy}^T\right]^T$ respectively. Since we wish all the derivative estimates to satisfy the irrotationality constraints, these terms are weighted by hyperparameters β_1, β_2, respectively, and are introduced by means of a $1-$norm due to the observation that violations of the irrotationality constraint tend to be sparsely distributed.
- The final two terms account for consistency of derivatives; the first one weighted by μ_1 compares the numerical second order derivatives with estimated ones, and the second one weighted by μ_2 promotes the equality of mixed derivatives.

The objective function can be understood in the following way; the first two terms correspond to data consistency, since the terms $\mathbf{b}_f, \mathbf{b}_g$ come from the input wrapped map, the next two terms impose total variation regularization, the two terms after that impose irrotationality constraints, and the final two terms are derivative consistency terms as already mentioned. Thus, Eq. 7 minimizes an objective that satisfies all the above-mentioned requirements to return derivative estimates that are consistent, and hence can be integrated over. The above minimization problem is readily formulated and solved in an alternating direction method of multipliers (ADMM) framework [35] (see Appendix D for more details).

E. Intelligent integration of derivatives

While the previous subsection focused on estimating the derivatives of the phase map, we now proceed to estimate the unwrapped phase map, denoted by $\hat{f}$. This is obtained by an integration of the solutions $\hat{f}_x, \hat{f}_y$, obtained from solving Eq. 7, followed by converting them to 2D maps from their vectorized versions. Instead of the usual $x-$, $y-$ raster scanning that is used for integration, we use a different method inspired by [36], where the integration of derivatives can be thought of a minimum spanning tree (MST) problem, with each pixel as a node, and absolute values of derivatives as edge weights. However, $\hat{f}_x, \hat{f}_y$ may still not be integrable at all pixels due to a violation of the irrotationality constraint. Thus the procedure to obtain $\hat{f}$ is outlined as follows:

1) Compute 2×2 loop summations of the derivative estimates $(\hat{f}_x, \hat{f}_y)$ at all points (also called "residues" [8]), i.e.

$$\hat{f}_x(i,j) + \hat{f}_y(i,j+1) - \hat{f}_x(i+1,j) - \hat{f}_y(i,j).$$

2) Points where this summation magnitude is greater than a (small) fixed threshold ϵ are considered to have inconsistent derivatives, and hence the associated 4 edges, i.e. : $(i,j) \rightarrow (i,j+1)$, $(i,j+1) \rightarrow (i+1,j+1)$, $(i+1,j+1) \rightarrow (i+1,j)$, $(i+1,j) \rightarrow (i,j)$ are removed from the integration routine.
3) Compute a minimum spanning tree with the remaining nodes; this gives an integration path for the derivative estimates.
4) In case a point is inaccessible (due to all associated edges being removed) then no integration value is assigned here. After integration involving the other nodes is complete, the missing values are later filled in by performing bilinear interpolation between neighboring values.

The above idea of "masking" out nodes where irrotationality does not hold is similar in essence to that of the use of quality maps in InSAR phase unwrapping techniques [1]; here, the information of the signal magnitude (that can accompany the wrapped phase information if recorded), helps in marking low quality areas of a phase map that should be masked out for the process of phase unwrapping; many other metrics for generating quality maps are also possible [37].

F. Iterative unwrapping of residual phase maps

The estimate obtained after solving Eq. 7 and performing intelligent integration may still contain errors due to noise. This can be readily checked by examining the residual map, f_{res}, defined as:

$$f_{res} = W[W[f] - \hat{f}] \tag{8}$$

This article has been accepted for publication in a future issue of this journal, but has not been fully edited. Content may change prior to final publication. Citation information: DOI 10.1109/TGRS.2021.3128565, IEEE Transactions on Geoscience and Remote Sensing

where $W[f]$ is the noisy wrapped input map, and $f, \hat{f}$ correspond to the true and estimated phase maps, respectively. If the unwrapping is perfect, there should be no 2π phase jumps in the residual map. These jumps can be readily estimated by counting the number of pixels having large magnitudes (nearly 2π) in the gradient maps of f_{res}. If the residual map does have significant 2π jumps, it means that the unwrapping result is inaccurate. However, one can continue to perform the unwrapping technique on the residual map to obtain an unwrapped estimate of the residual map, and add that to the initial unwrapped estimate (as demonstrated in [14]). This insight suggests that better estimates can be obtained by iterative unwrapping of the residuals, and simply summing up all of those estimates (See Appendix E for a detailed explanation).

G. Novel 2D phase unwrapping method summary

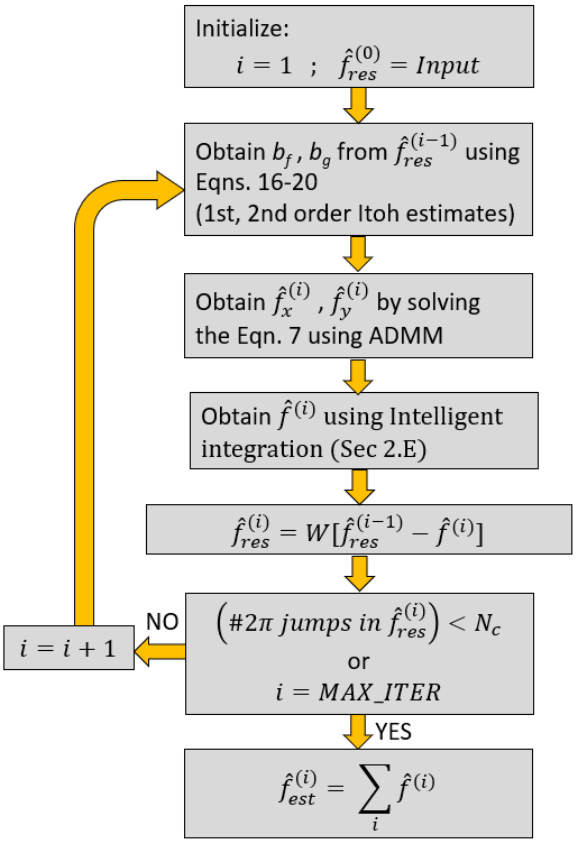

Fig. 3: Flowchart depicting the phase unwrapping procedure

We summarize the entire phase unwrapping algorithm in Fig. 3, which involves iterative unwrapping of residual wrapped phase maps, with each iteration invoking Eq. (7) to estimate the derivatives and using intelligent integration as previously outlined. In order to better understand the impact of adding second order information to our phase unwrapping algorithm, we study and analyse the results of the minimization problem in Eq. 7 for two separate cases[1]

1) **ITV:** $\epsilon_2 = 0, \mu_1 = 0, \mu_2 = 0, \lambda_2 = 0, \beta_2 = 0$
Here, we do not use any 2nd order information, and instead work with the first order Itoh estimates [38]. Additionally, for any 2D map h, total variation regularization is implemented as a sum of a simple anisotropic norm, given by:

$$\|D_x\mathbf{h}\|_1 + \|D_y\mathbf{h}\|_1,$$

where D_x, D_y are first-order forward difference operators in the x, y directions, respectively. The third term in Eq. 7 thus becomes:

$$\begin{aligned}\mathrm{TV}(\mathbf{f}) &= \mathrm{TV}(\left[\mathbf{f}_x^T, \mathbf{f}_y^T\right]^T) \\ &= (\|D_x\mathbf{f}_x\|_1 + \|D_y\mathbf{f}_x\|_1) + (\|D_x\mathbf{f}_y\|_1 + \|D_y\mathbf{f}_y\|_1).\end{aligned}$$

2) **ITVC:** This case considers the minimization problem of Eq. 7 in its full, general sense with a combined use of first and second order information; therefore all hyperparameters are non-zero. TV regularization creates piece-wise constant solutions, also known as the *staircase effect* in image restoration. Since it is desirable to estimate smoother solutions, we take inspiration from [32] and make the third term in Eq. 7 be a higher-order anisotropic TV norm (instead of a simple 1st order TV norm) given by:

$$\|D_{xx}\mathbf{h}\|_1 + \|D_{xy}\mathbf{h}\|_1 + \|D_{yx}\mathbf{h}\|_1 + \|D_{yy}\mathbf{h}\|_1$$

where $D_{xx}, D_{xy}, D_{yx}, D_{yy}$ are second-order forward difference operators. The fourth term in Eq. 7 remains a simple anisotropic TV norm.

In the next Section, we show numerical results pertaining to these methods.

III. Results

A. Simulation experiments

To test the proposed methods, realistic synthetic terrain data was generated [2]. To test out claims about the usability of the approaches in different sampling settings, synthetic data maps were downsampled by a factor of $4\times$ (in each direction), thereby giving two types of maps - finely sampled, and coarse sampled. Fig. 4 illustrates one of the many synthetic maps generated, along with the wrapped versions of the fine and coarse sampling scenarios.

Unwrapping procedures of ITV, and ITVC were performed on the wrapped noisy versions of these maps, for a maximum of 5 iterations, with the hyperparameters $(\epsilon_1, \epsilon_2, \lambda_1, \lambda_2, \beta_1, \beta_2, \mu_1, \mu_2)$ being set to $(1, 0, 1, 0, 1000, 0, 0, 0)$ for ITV and $(1, 1, 1, 1, 1000, 1000, 1, 1)$ for ITVC (the hyper-parameters values are chosen empirically via a grid search). The

[1]The nomenclature of these methods arises by translating **I** as irrotationality preserving, **TV** as total variation regularization, and **C** as combined first and second order utilization.

[2]Tucker McClure (2021). Automatic Terrain Generation https://www.mathworks.com/matlabcentral/fileexchange/39559-automatic-terrain-generation, MATLAB Central FileExchange.

This article has been accepted for publication in a future issue of this journal, but has not been fully edited. Content may change prior to final publication. Citation information: DOI 10.1109/TGRS.2021.3128565, IEEE Transactions on Geoscience and Remote Sensing

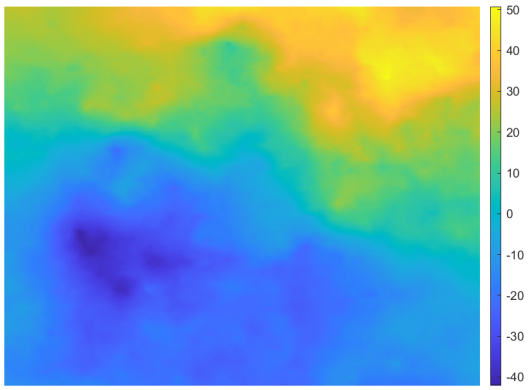

(a) Synthetic terrain map (absolute phase) of 256×256 pixels

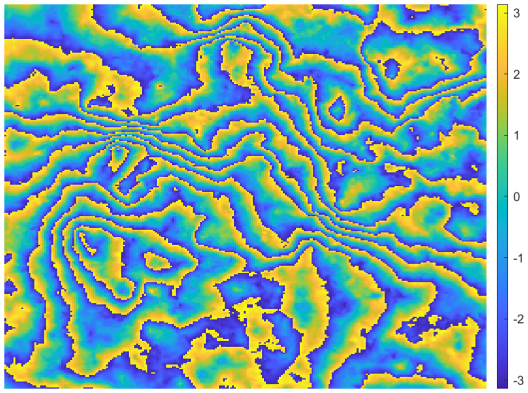

(b) Wrapped map (fine sampled case, 256×256)

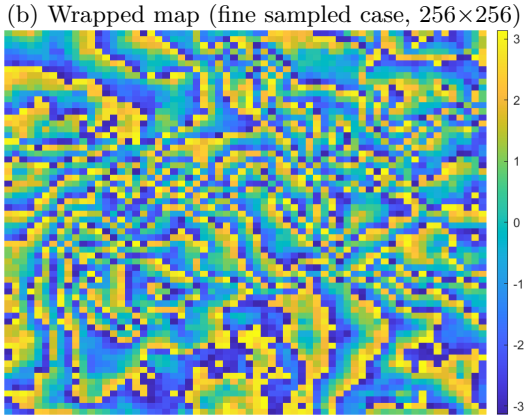

(c) Wrapped map (coarse sampled case, 64×64)

Fig. 4: Illustration of synthetic phase maps generated

threshold, N_C, for the total number of 2π jumps permissible in any residual map being set to 2% of the total number of pixels, following the algorithm described in the flowchart in Fig. 3. To consider the effects of noise, Gaussian noise was added to the true unwrapped phase maps prior to the wrapping operation, so as to simulate noisy wrapped phase maps. Gaussian noise with standard deviations equalling $\pi/6$ and $\pi/4$ were added to the maps. To judge the quality of unwrapping, we used the mean absolute error (MAE) as a metric, along with two popular metrics to quantify image quality, namely the Feature SIMilarity (FSIM) [39] and the Maximum Local Variation (MLV) sharpness [40]. Judging the quality of an image is difficult — particularly in relation to fine structure detail — by the mean absolute error value. Hence, looking at FSIM and MLV sharpness metrics provides useful insight with regard to the unwrapping quality. The implementations for FSIM and MLV metrics were taken from the respective author code releases[3]. We note an important distinction between the above metrics; MAE and FSIM require knowledge of the reference image, whereas MLV is reference free.

The unwrapping results of ITV, ITVC, were compared alongside the PUMA unwrapping method [17]. The hyper-parameter chosen for the implementation[4] was the clique potential exponent $m = 1$. The comparison was done in a Monte Carlo fashion – 60 synthetic maps were generated (both fine and coarse sampling) – and the ITV, ITVC, and PUMA unwrappings were performed on each of these maps. In the next Subsection, we present results averaged over this set of experiments.

B. Results on synthetic terrains

We first report the ablation experiments performed to study the impact of each of the two regularizing terms (total variation and irrotationality), as well as the impact of multiple iterations (we consider upto 5 in total). The data fidelity and consistency terms are retained in all the experiments ($\epsilon_1 = \epsilon_2 = \mu_1 = \mu_2 = 1$). These experiments are: "Base" (i.e. $\lambda_1 = \lambda_2 = \beta_1 = \beta_2 = 0$), "TV-only" (i.e. $\beta_1 = \beta_2 = 0$), "IRR-only (i.e. $\lambda_1 = \lambda_2 = 0$) and "Full" (i.e. all hyper-parameters considered) and are detailed in Table I. It is seen that: (i) irrotationality has a higher impact compared to the total variation regularization, (ii) iterative phase unwrapping is crucial in arriving at the best solution, and (iii) using all the terms introduced in Eq. 7 is required for obtaining the best unwrapping results.

Ablation Experiment	First iteration	Final iteration
Base	16.4 rad	16.8 rad
TV-only	14.0 rad	13.0 rad
IRR-only	10.7 rad	6.8 rad
Full	10.7 rad	5.9 rad

TABLE I: Average MAE (radians) for unwrapping results for 60 different simulated wrapped maps (coarsely-sampled, and with $\pi/6$ noise level)

We report the average percentage increase in FSIM, MLV, and MAE values *with respect to* the ITV unwrapping result. This helps us analyse the relative performance of ITVC and PUMA with respect to ITV, and thus, helps in comparing the performance of all the methods.

The first significant set of results are presented reporting the average increase in using ITVC or PUMA over ITV is summarized in Table II for low noise, and in Table

[3]FSIM taken from https://www4.comp.polyu.edu.hk/~cslzhang/IQA/FSIM/FSIM.htm, author L Zhang; MLV taken from https://www.mathworks.com/matlabcentral/fileexchange/49991-maximum-local-variation-mlv-code-for-sharpness-assessment-of-imag, author Khosro Bahrami.

[4]The implementation was adapted from the publicly available resource at: http://www.lx.it.pt/~bioucas/code.htm

This article has been accepted for publication in a future issue of this journal, but has not been fully edited. Content may change prior to final publication. Citation information: DOI 10.1109/TGRS.2021.3128565, IEEE Transactions on Geoscience and Remote Sensing

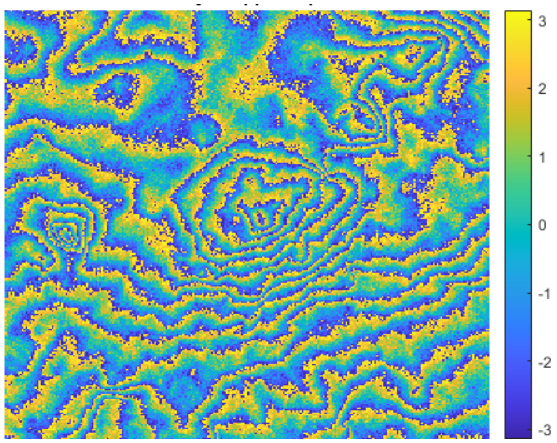

(a) Fine sampled case (256×256)

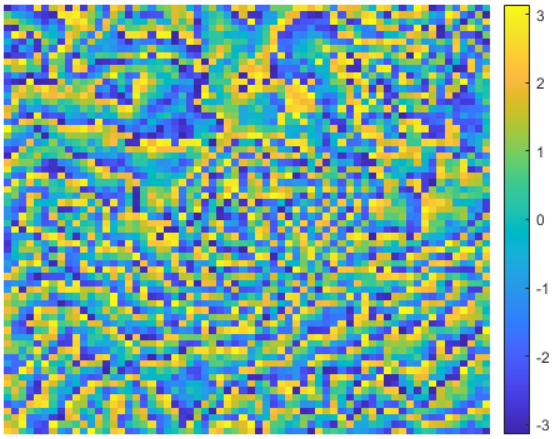

(b) Coarse sampled case (64×64)

Fig. 5: Noisy input wrapped maps used

	Fine maps		Coarse maps	
	ITVC	PUMA	ITVC	PUMA
Avg. MAE increase	14%	−42%	−9%	12%
Avg. FSIM increase	0.58%	0.30%	2.0%	1.2%
Avg. MLV increase	2%	−6%	18%	37%

TABLE II: Avg. metric increase w.r.t. the ITV unwrapping result for $\frac{\pi}{6}$ noise case. For MAE - lower is better; for FSIM/MLV - higher is better.

	Fine maps		Coarse maps	
	ITVC	PUMA	ITVC	PUMA
Avg. MAE increase	10%	−68%	−3.9%	14.1%
Avg. FSIM increase	1.2%	1.5%	1.8%	0.85%
Avg. MLV increase	8.8%	−1.7%	8%	57%

TABLE III: Avg. metric increase w.r.t. the ITV unwrapping result for $\frac{\pi}{4}$ noise case. For MAE - lower is better; for FSIM/MLV - higher is better.

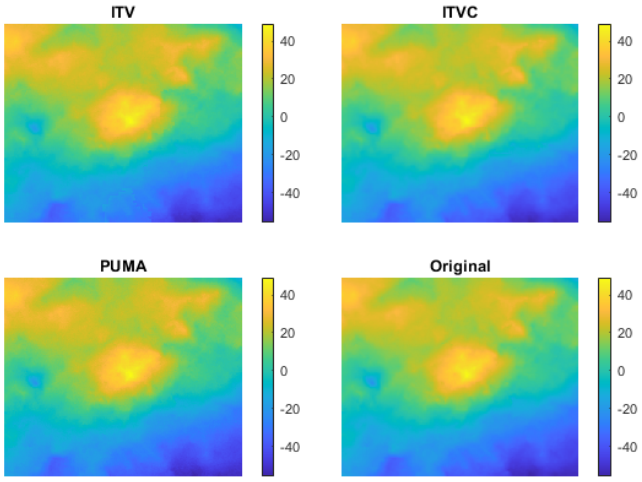

Fig. 6: Unwrapping results on a finely sampled synthetic terrain ($\pi/6$ noise)

III for higher noise. Since one wishes for lower error, a negative increase (i.e. decrease) is desirable to the MAE metric, while a higher, positive increase highlights better performance in terms of FSIM and MLV metric. Note that these are results obtained from the Monte Carlo averaging over all datasets used.

To better appreciate the visual quality of unwrapping, we present graphics of the unwrapping for one representative map in the dataset as seen in Figs. 5, 6, 7 for $\pi/6$-level noise for both fine and coarse maps. Fig. 7 illustrates how ITVC is superior at mapping structures as compared to the PUMA result for coarse maps, while the performance on fine maps is competitive. We also considered the case of applying an iterative procedure to the PUMA algorithm. We note that doing so leads to better phase unwrapping (more so at lower noise), as compared to a one-shot unwrapping. However, we note that despite this measure, the proposed method still outperforms iterative PUMA for all noise levels on coarsely sampled maps.

C. Real data experiments

To test the proposed methods on real world data, interferometric synthetic aperture radar (InSAR) data [41] from the Alaska Satellite Facility (ASF[5]) was used, and a wrapped phase map located roughly over a location in Hawaii was obtained. We consider two cropped terrain maps derived from the above, which are overlapping ones. The first is a cropped region downsampled by 8× (along each axis) (see Fig. 8) with respect to the original map. This downsampling still retains the fine structures of the map, enough to consider the map as finely sampled. The second is the same cropped region downsampled by 64× (along each axis, see Fig. 9), to simulate a coarse wrapped map. The two maps are overlapping and thus refer to the same features on the ground. Unwrapping results can be seen in Fig. 10 for all the three proposed methods.

[5]https://www.asf.alaska.edu/

This article has been accepted for publication in a future issue of this journal, but has not been fully edited. Content may change prior to final publication. Citation information: DOI 10.1109/TGRS.2021.3128565, IEEE Transactions on Geoscience and Remote Sensing

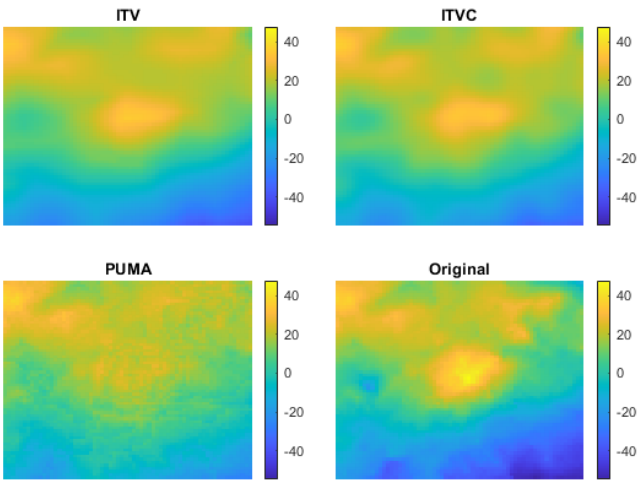

Fig. 7: Unwrapping results on a coarsely sampled terrain ($\pi/6$ noise)

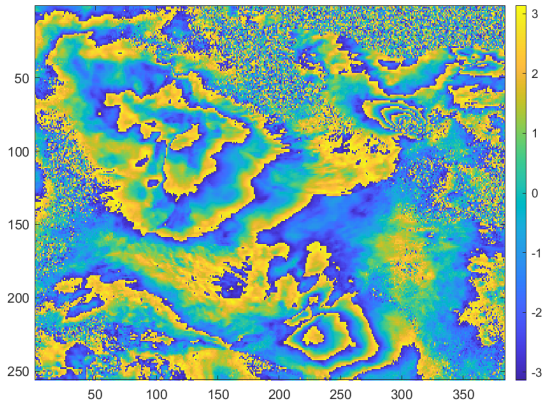

Fig. 8: Real map #1. Cropped region of InSAR map, downsampled by 8× (256×384 pixels) Source: [41]

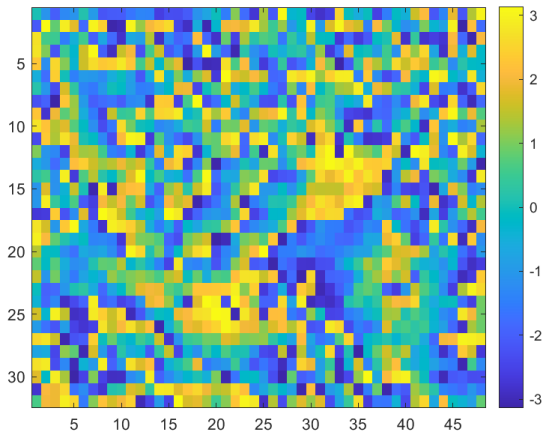

Fig. 9: Real map #2. Cropped region of InSAR map, downsampled by 64× (32×48 pixels) Source: [41]

IV. Conclusion

Based on our extensive numerical studies on both synthetic and real-world data, we can summarize our results and findings as follows.

On image quality and noise-related performance

1) From the simulation results on synthetic terrain data, it is clear that ITVC performs better than the ITV method in both FSIM and MLV sharpness metrics, for both noise levels, and for both the sampling scenarios. Particularly for coarse sampling, ITVC has better MAE, FSIM, and MLV performance, for both noise levels. This can be justified as the ITV method uses only first order TV regularization, and hence the unwrappings are smoother and do not capture fine structures, as is seen in Figs. 6-7.
2) The difference in unwrapping quality is more pronounced for the low noise scenario, which can be justified theoretically. It can be shown that a higher noise level in the signal implies a higher noise in the signal's first order derivatives, and an even higher noise in the second order derivatives. Thus, for higher noise scenarios, there is a greater chance of violation of the assumption for second order Itoh estimates, compared to the first order Itoh estimates' assumption. This insight suggests a diminishing return for using higher order Itoh estimate information, and is seen in our results as well – the performance improvement seen with ITVC over ITV is less for the $\pi/4$ noise level compared to the $\pi/6$ noise level case.

On unwrapping coarse v/s fine phase maps

1) Considering the synthetic terrain experiments, we observe that for the fine sampling case, PUMA outperforms ITV and ITVC as seen distinctly by looking at the MAE metric, suggesting suitability of PUMA for finely sampled phase maps. However, for the coarse sampling case it is seen that ITVC is clearly *better suited* in comparison to both ITV and PUMA. Even though PUMA results how a higher MLV, visual inspection shows that the ITVC result is superior, and thus the enhanced sharpness index is possibly due to a artificially jagged unwrapping result.
2) For the InSAR experiments, we consider the unwrapping of a fine and coarsely sampled wrapped phase map of the same region. By a visual inspection of the unwrapping, we *assign* the PUMA unwrapping result for the finely sampled map as the *reference*. The unwrapping results from the ITV and PUMA procedures for the finely sampled map seem to be of similar quality, while ITVC shows a few unwrapping errors near the top edge of the map (see Boxes A in Fig. 10).
3) In the case of the coarsely sampled map, ITVC unwrapping show finer details and structures as compared to ITV. The PUMA unwrapping result looks noisier and less smooth. Certain small structures, such as the depression at the bottom edge of the map are missed in the PUMA result, while retained in ITVC (see Boxes B in Fig. 10). Moreover, PUMA unwrapping of the vertically aligned hill close to

This article has been accepted for publication in a future issue of this journal, but has not been fully edited. Content may change prior to final publication. Citation information: DOI 10.1109/TGRS.2021.3128565, IEEE Transactions on Geoscience and Remote Sensing

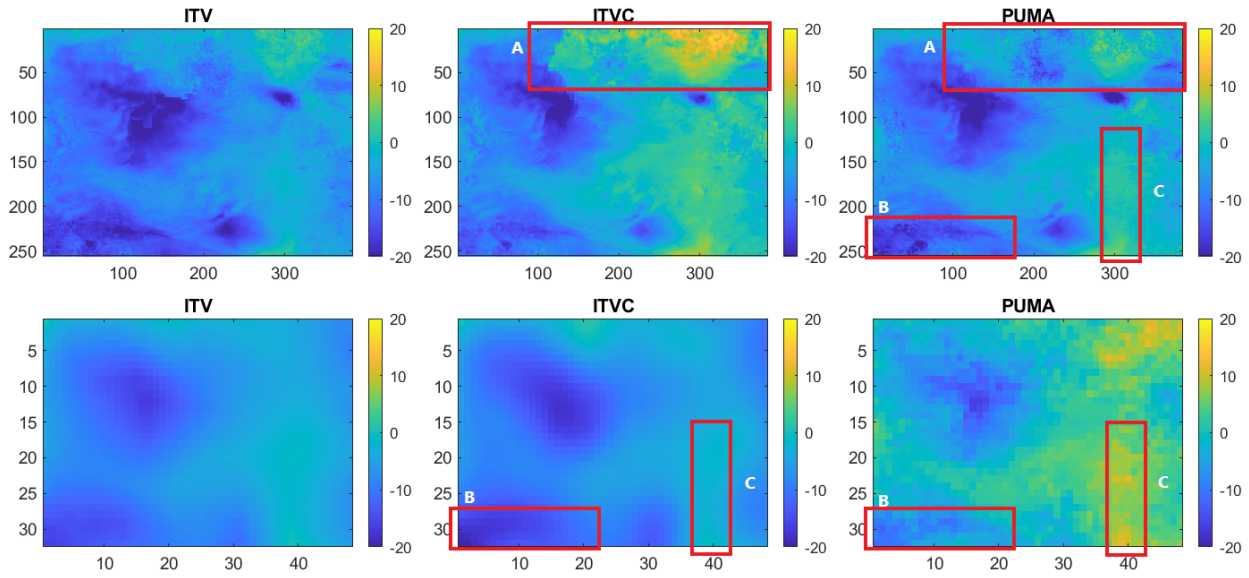

Fig. 10: Results on: finely sampled map (top row), coarsely sampled map (bottom row). The PUMA unwrapping result (top-right) is considered as reference when comparing unwrapping results across the fine and coarse maps. With that as reference, different boxes highlight the differences in unwrapping. Box A shows that ITVC has slight errors in unwrapping in the fine sampled case. Whereas boxes B and C show that ITVC performs better that PUMA in the coarse sampled case.

the bottom-right corner seems to be incorrect, while ITVC and ITV unwrappings seem to have a similar phase value compared to the reference (see Boxes C in Fig. 10). This is in accordance with our simulation results, which show that for coarse maps, ITVC has a lower unwrapping error, and also better mapping of structures compared to PUMA.

In closing, we remark that the overall philosophy of the higher order Itoh conditions, i.e. unwrapping the n-order derivatives according to the $n+1$-order derivatives, can also be incorporated in traditional phase unwrapping methods. Care must be taken to ensure that the consistency relations mentioned below are respected while unwrapping. These are (i) equality of the gradient of the n-order derivative estimate with the $n+1$-order derivative estimate, and (ii) equality of mixed higher order derivatives; these are also the last two terms of the objective function in our approach.

In summary, our proposed algorithm excels at phase unwrapping on coarsely sampled phase maps as compared to some of the contemporary algorithms considered, and is thus a compelling candidate for an upcoming set of applications that desire low resolution images.

References

[1] D. C. Ghiglia and M. D. Pritt, *Two-dimensional phase unwrapping: theory, algorithms, and software*, vol. 4. Wiley New York, 1998.

[2] L. C. Graham, "Synthetic interferometer radar for topographic mapping," *Proceedings of the IEEE*, vol. 62, no. 6, pp. 763–768, 1974.

[3] H. A. Zebker and R. M. Goldstein, "Topographic mapping from interferometric synthetic aperture radar observations," *Journal of Geophysical Research: Solid Earth*, vol. 91, no. B5, pp. 4993–4999, 1986.

[4] M. Takeda, H. Ina, and S. Kobayashi, "Fourier-transform method of fringe-pattern analysis for computer-based topography and interferometry," *JosA*, vol. 72, no. 1, pp. 156–160, 1982.

[5] S. Grilli, P. Ferraro, S. De Nicola, A. Finizio, G. Pierattini, and R. Meucci, "Whole optical wavefields reconstruction by digital holography," *Optics Express*, vol. 9, no. 6, pp. 294–302, 2001.

[6] H. Yu, Y. Lan, Z. Yuan, J. Xu, and H. Lee, "Phase unwrapping in insar: A review," *IEEE Geoscience and Remote Sensing Magazine*, vol. 7, no. 1, pp. 40–58, 2019.

[7] K. Itoh, "Analysis of the phase unwrapping algorithm," *Applied optics*, vol. 21, no. 14, pp. 2470–2470, 1982.

[8] R. M. Goldstein, H. A. Zebker, and C. L. Werner, "Satellite radar interferometry: Two-dimensional phase unwrapping," *Radio science*, vol. 23, no. 4, pp. 713–720, 1988.

[9] D. Zheng and F. Da, "A novel algorithm for branch cut phase unwrapping," *Optics and Lasers in Engineering*, vol. 49, no. 5, pp. 609–617, 2011.

[10] N. H. Ching, D. Rosenfeld, and M. Braun, "Two-dimensional phase unwrapping using a minimum spanning tree algorithm," *IEEE Transactions on Image Processing*, vol. 1, no. 3, pp. 355–365, 1992.

[11] H. Yu, M. Xing, and Z. Bao, "A fast phase unwrapping method for large-scale interferograms," *IEEE transactions on geoscience and remote sensing*, vol. 51, no. 7, pp. 4240–4248, 2013.

[12] D. C. Ghiglia and L. A. Romero, "Minimum l_p-norm two-dimensional phase unwrapping," *JOSA A*, vol. 13, no. 10, pp. 1999–2013, 1996.

[13] M. Costantini, "A novel phase unwrapping method based on network programming," *IEEE Transactions on geoscience and remote sensing*, vol. 36, no. 3, pp. 813–821, 1998.

[14] H. Y. Huang, L. Tian, Z. Zhang, Y. Liu, Z. Chen, and G. Barbastathis, "Path-independent phase unwrapping using phase gradient and total-variation (tv) denoising," *Optics express*, vol. 20, no. 13, pp. 14075–14089, 2012.

[15] H. Yu, Y. Lan, H. Lee, and N. Cao, "2-d phase unwrapping using minimum infinity-norm," *IEEE Geoscience and Remote Sensing Letters*, vol. 15, no. 12, pp. 1887–1891, 2018.

[16] C. W. Chen and H. A. Zebker, "Two-dimensional phase unwrapping with use of statistical models for cost functions in nonlinear optimization," *JOSA A*, vol. 18, no. 2, pp. 338–351, 2001.

[17] J. M. Bioucas-Dias and G. Valadao, "Phase unwrapping via graph cuts," *IEEE Transactions on Image processing*, vol. 16, no. 3, pp. 698–709, 2007.

[18] J. Zhang, X. Tian, J. Shao, H. Luo, and R. Liang, "Phase unwrapping in optical metrology via denoised and convolutional segmentation networks," *Optics express*, vol. 27, no. 10, pp. 14903–14912, 2019.
[19] L. Zhou, H. Yu, and Y. Lan, "Deep convolutional neural network-based robust phase gradient estimation for two-dimensional phase unwrapping using sar interferograms," *IEEE Transactions on Geoscience and Remote Sensing*, vol. 58, no. 7, pp. 4653–4665, 2020.
[20] G. Dardikman-Yoffe, D. Roitshtain, S. K. Mirsky, N. A. Turko, M. Habaza, and N. T. Shaked, "Phun-net: ready-to-use neural network for unwrapping quantitative phase images of biological cells," *Biomedical optics express*, vol. 11, no. 2, pp. 1107–1121, 2020.
[21] F. Sica, F. Calvanese, G. Scarpa, and P. Rizzoli, "A cnn-based coherence-driven approach for insar phase unwrapping," *IEEE Geoscience and Remote Sensing Letters*, 2020.
[22] L. Zhou, H. Yu, Y. Lan, and M. Xing, "Deep learning-based branch-cut method for insar two-dimensional phase unwrapping," *IEEE Transactions on Geoscience and Remote Sensing*, 2021.
[23] M. A. Remy, K. A. de Macedo, and J. R. Moreira, "The first uav-based p-and x-band interferometric sar system," in *2012 IEEE International Geoscience and Remote Sensing Symposium*, pp. 5041–5044, IEEE, 2012.
[24] L. Moreira, F. Castro, J. A. Góes, L. Bins, B. Teruel, J. Fraccarolli, V. Castro, M. Alcântara, G. Oré, D. Luebeck, *et al.*, "A drone-borne multiband dinsar: Results and applications," in *2019 IEEE Radar Conference (RadarConf)*, pp. 1–6, IEEE, 2019.
[25] S. Xia, Y. Huang, S. Peng, Y. Wu, and X. Tan, "Robust phase unwrapping for phase images in fourier domain doppler optical coherence tomography," *Journal of biomedical optics*, vol. 22, no. 3, p. 036014, 2017.
[26] D. Parshall and M. K. Kim, "Digital holographic microscopy with dual-wavelength phase unwrapping," *Applied Optics*, vol. 45, no. 3, pp. 451–459, 2006.
[27] D. N. Breslauer, R. N. Maamari, N. A. Switz, W. A. Lam, and D. A. Fletcher, "Mobile phone based clinical microscopy for global health applications," *PloS one*, vol. 4, no. 7, p. e6320, 2009.
[28] T. Aidukas, R. Eckert, A. R. Harvey, L. Waller, and P. C. Konda, "Low-cost, sub-micron resolution, wide-field computational microscopy using opensource hardware," *Scientific reports*, vol. 9, no. 1, pp. 1–12, 2019.
[29] R. Chartrand, "Numerical differentiation of noisy, nonsmooth data," *International Scholarly Research Notices*, vol. 2011, 2011.
[30] L. I. Rudin and S. Osher, "Total variation based image restoration with free local constraints," in *Proceedings of 1st International Conference on Image Processing*, vol. 1, pp. 31–35, IEEE, 1994.
[31] G. Ferraioli, A. Shabou, F. Tupin, and V. Pascazio, "Multichannel phase unwrapping with graph cuts," *IEEE Geoscience and Remote Sensing Letters*, vol. 6, no. 3, pp. 562–566, 2009.
[32] X.-G. Lv, Y.-Z. Song, S.-X. Wang, and J. Le, "Image restoration with a high-order total variation minimization method," *Applied Mathematical Modelling*, vol. 37, no. 16-17, pp. 8210–8224, 2013.
[33] R. Guo, W. Zhang, R. Liu, C. Duan, and F. Wang, "Phase unwrapping in dual-wavelength digital holographic microscopy with total variation regularization," *Optics letters*, vol. 43, no. 14, pp. 3449–3452, 2018.
[34] A. Agrawal, R. Raskar, and R. Chellappa, "What is the range of surface reconstructions from a gradient field?," in *European conference on computer vision*, pp. 578–591, Springer, 2006.
[35] S. Boyd, N. Parikh, and E. Chu, *Distributed optimization and statistical learning via the alternating direction method of multipliers*. Now Publishers Inc, 2011.
[36] A. Agrawal, R. Chellappa, and R. Raskar, "An algebraic approach to surface reconstruction from gradient fields," in *Tenth IEEE International Conference on Computer Vision (ICCV'05) Volume 1*, vol. 1, pp. 174–181, IEEE, 2005.
[37] G. Liu, R. Wang, Y. Deng, R. Chen, Y. Shao, and Z. Yuan, "A new quality map for 2-d phase unwrapping based on gray level co-occurrence matrix," *IEEE Geoscience and Remote Sensing Letters*, vol. 11, no. 2, pp. 444–448, 2013.
[38] B. Ghanekar, D. Narayan, and U. Khankhoje, "An irrotationality preserving total variation algorithm for phase unwrapping," in *2018 Twenty Fourth National Conference on Communications (NCC)*, pp. 1–6, IEEE, 2018.
[39] L. Zhang, L. Zhang, X. Mou, and D. Zhang, "Fsim: A feature similarity index for image quality assessment," *IEEE transactions on Image Processing*, vol. 20, no. 8, pp. 2378–2386, 2011.
[40] K. Bahrami and A. C. Kot, "A fast approach for no-reference image sharpness assessment based on maximum local variation," *IEEE Signal Processing Letters*, vol. 21, no. 6, pp. 751–755, 2014.
[41] https://www.asf.alaska.edu/ASF DAAC 2018, contains modified http://www.esa.int/Our_Activities/Observing_the_Earth/CopernicusCopernicus Sentinel data, 2018, processed by ESA.

Appendix A
Proof for Theorem 1

Given a sequence x_n and a wrapping operator W:

$$W(x_n) = x_n + 2\pi k_n \quad (k_n \in \mathbb{Z}) \tag{9}$$

Thus,

$$W(\Delta_m(w_n)) = \Delta_m(w_n) + 2\pi l_n \tag{10}$$
$$W(\Delta_m(w_n)) = \Delta_m(x_n) + 2\pi(\Delta_m(k_n) + l_n) \tag{11}$$
$$W(\Delta_m(w_n)) = \Delta_m(x_n) + 2\pi(l_n + \Delta_m(k_n)) \tag{12}$$

Note that $W(\Delta_m(w_n)) \in [-\pi, \pi)$ and $(l_n + \Delta_m(k_n)) \in \mathbb{Z}$. Hence, if we have $\Delta_m(x_n) \in (-\pi, \pi)$, this implies that $(l_n + \Delta_m(k_n)) = 0$, which implies that

$$W(\Delta_m(w_n)) = \Delta_m(x_n). \tag{13}$$

Appendix B
Higher order Itoh condition in 2D

In this Section, we provide details for the two-dimensional (2D) extensions of the higher order Itoh conditions [1]. Given a 2D signal, $f \in \mathbb{R}^{M\times N}$, we define derivative maps with the forward x, y difference operators denoted by $\Delta_x f \in \mathbb{R}^{M\times N-1}$ and $\Delta_y f \in \mathbb{R}^{M-1\times N}$ -

$$\Delta_x f(i,j) = f(i,j+1) - f(i,j) \tag{14}$$
$$\Delta_y f(i,j) = f(i+1,j) - f(i,j), \tag{15}$$

where M, N denote the height and width of the signal, respectively.

The 2D Itoh condition then states that:

$$W[\Delta_x W[f]] = \Delta_x f, \text{ if } |\Delta_x f| < \pi, \tag{16}$$
$$W[\Delta_y W[f]] = \Delta_y f, \text{ if } |\Delta_y f| < \pi. \tag{17}$$

This fact has been used in several works for the task of 2D phase unwrapping [13], [14].

Extending the above discussion towards higher order Itoh conditions, specifically for $m = 2$, we note the following consequences of Theorem 1 to 2D signals for a phase map f:

$$W[\Delta_{xx} W[f]] = \Delta_{xx} f, \text{ if } |\Delta_{xx} f| < \pi, \tag{18}$$
$$W[\Delta_{yy} W[f]] = \Delta_{yy} f, \text{ if } |\Delta_{yy} f| < \pi, \tag{19}$$
$$W[\Delta_{xy} W[f]] = W[\Delta_{yx} W[f]] = \Delta_{xy} f = \Delta_{yx} f \quad \text{if } |\Delta_{xy} f| < \pi. \tag{20}$$

The proof for the above statement is trivial - one can apply the one-dimensional higher order Itoh condition to each direction x and y independently.

This article has been accepted for publication in a future issue of this journal, but has not been fully edited. Content may change prior to final publication. Citation information: DOI 10.1109/TGRS.2021.3128565, IEEE Transactions on Geoscience and Remote Sensing

Appendix C
Proof of Theorem 2

Let us define the higher order derivative sequence, $\{h[n]\}$, in terms of the lower order derivative sequence (of length N), $\{g[n]\}$, by means of a finite difference:

$$h[n] = g[n] - g[n-1],\ 2 \leq n \leq N. \tag{21}$$

We may treat $g[n]$ as a random variable in general, but $g[n], g[n-1]$ are not independent random variables since the surface is expected to demonstrate spatial correlation (this is our definition of "reasonably smooth"). Simplifying the notation as $z : h[n]$, $x : g[n]$ and $y : g[n-1]$, we seek the probability distribution function (PDF) of $z = x - y$. For this, we need the joint PDF, p_{xy}, of correlated random variables, x, y. Assuming both x, y can be modelled as gaussian random variables of zero mean and variance σ^2, and with a correlation coefficient ρ, we get:

$$p_{xy}(x,y) = \exp\left(-\frac{x^2+y^2-2\rho xy}{2(1-\rho^2)\sigma^2}\right) / \left(2\pi\sigma^2\sqrt{1-\rho^2}\right) \tag{22}$$

Our empirical observations in the form of histograms in Figs. 1(b,c) support the modelling of x, y as gaussian random variables. From here, the cummulative distribution function (CDF) of z, can be estimated by integrating Eq. (22) over a region defined as $D : \{x, y | x - y < z\}$. Next, we obtain the PDF of z by differentiating this CDF, and find that z also has a gaussian PDF with zero mean and variance $\sigma_z^2 = \sigma^2(2-2\rho)$. Thus, as long as adjacent points on the terrain are correlated with a correlation coefficient greater than $\frac{1}{2}$, we will have $\sigma_z < \sigma$. From here, we compute our required probabilities as:

$$P(|x| > \pi) = 1 - \int_{-\pi}^{\pi} \frac{\exp[-\frac{x^2}{2\sigma^2}]}{2\pi\sigma} = 1 - \text{erf}(\frac{\pi}{\sqrt{2}\sigma}) = C, \tag{23}$$

and similarly,

$$P(|z| > \pi) = 1 - \text{erf}(\frac{\pi}{\sqrt{2}\sigma_z}) < C, \tag{24}$$

where the final inequality follows due to the monotonic increasing nature of the erf() function when $\sigma_z < \sigma$.

Appendix D
ADMM Formulation

In the following section, we outline the ADMM formulation of the optimization problem given in Eq. 7. For sake of brevity and simplicity, we will discuss the ITVC case ($\epsilon_1 = \epsilon_2 = 1$), and with $\lambda_1 = \lambda_2 = \lambda$, $\beta_1 = \beta_2 = \beta$, and $\mu_1 = \mu_2 = \mu$.

Firstly we note that Eq. 7 can be expressed as -

$$\left\| A \begin{bmatrix} \mathbf{f} \\ \mathbf{g} \end{bmatrix} - \tilde{\mathbf{b}} \right\|_2^2 + \lambda \left\| B \begin{bmatrix} \mathbf{f} \\ \mathbf{g} \end{bmatrix} \right\|_1^1 \tag{25}$$

where A, B are linear operators (matrices) and $\tilde{\mathbf{b}}$ is a vector, with

$$A = \begin{bmatrix} I & 0 \\ 0 & I \\ \sqrt{\mu}\nabla & -\sqrt{\mu}I \\ 0 & \begin{bmatrix} 0 & \sqrt{\mu}I & -\sqrt{\mu}I & 0 \end{bmatrix} \end{bmatrix},\ \tilde{\mathbf{b}} = \begin{bmatrix} \mathbf{b}_f \\ \mathbf{b}_g \\ 0 \\ 0 \end{bmatrix} \tag{26}$$

and

$$B = \begin{bmatrix} F_{HTV} & 0 \\ 0 & F_{TV} \\ \frac{\beta}{\lambda}M_1 & 0 \\ 0 & \frac{\beta}{\lambda}\begin{bmatrix} M_2 & 0 \\ 0 & M_3 \end{bmatrix} \end{bmatrix} \tag{27}$$

where F_{HTV} is the stack of HTV operators to applied on $\mathbf{f}_x$, $\mathbf{f}_y$; F_{TV} is the stack of TV operators to be applied on $\mathbf{g}_{xx}$, $\mathbf{g}_{xy}$, $\mathbf{g}_{yx}$, $\mathbf{g}_{yy}$; and M is the matrix depicting the irrotationality operator.

Let $\begin{bmatrix} \mathbf{f} & \mathbf{g} \end{bmatrix}^T = \tilde{\mathbf{f}}$. Thus, Eq. 7 can be written as

$$\begin{aligned} \underset{f,g}{\text{argmin}} \left\| A\tilde{\mathbf{f}} - \tilde{\mathbf{b}} \right\|_2^2 + \lambda \left\| \mathbf{z} \right\|_1^1 \\ \text{s.t. } B\tilde{\mathbf{f}} - \mathbf{z} = 0 \end{aligned} \tag{28}$$

The above expression is in the standard ADMM format [35], and the corresponding updates for the primal variables $\tilde{\mathbf{f}}$, $\mathbf{z}$ and the dual variable $\mathbf{u}$ are:

$$\tilde{\mathbf{f}}_{k+1} = (A^TA + \rho B^TB)^{-1}(\tilde{\mathbf{b}} + B^T(\rho\mathbf{z}_k - \mathbf{u}_k)) \tag{29}$$

$$\mathbf{z}_{k+1} = \mathcal{S}_{\lambda/\rho}(B\tilde{\mathbf{f}}_{k+1} + \mathbf{u}_k/\rho) \tag{30}$$

$$\mathbf{u}_{k+1} = \mathbf{u}_k + \rho(B\tilde{\mathbf{f}}_{k+1} - \mathbf{z}_{k+1}) \tag{31}$$

where $\mathcal{S}$ is the soft-thresholding operator. The matrices A, B are sparse, thus allowing for fast and efficient computations of the above updates.

Appendix E
Iterative unwrapping of residuals

Let $W[]$ denote the wrapping operator. Let $Unwrap(.)$ be a function that unwraps a wrapped phase map $W[f]$ (could be any method - ITV, ITVC, etc.). Let the first estimate be $f^{(1)} = Unwrap(W[f])$, and let $e^{(1)}$ denote the error between the true unwrapped map f and the estimate (namely $Unwrap(W[f])$). Let $f_{res}^{(1)} = W[W[f] - f^{(1)}]$, as per Eq. 8. We now proceed to show how addition of unwrapped estimates of residuals obtained iteratively lead to better estimation. We have

$$\begin{aligned} & f = Unwrap(W[f]) + e^{(1)} \\ \implies & f = f^{(1)} + e^{(1)} \\ \implies & f = f^{(1)} + Unwrap(W[e^{(1)}]) + e^{(2)} \\ \implies & f = f^{(1)} + Unwrap(W[f - f^{(1)}]) + e^{(2)} \\ \implies & f = f^{(1)} + Unwrap(W[W[f] - f^{(1)}]) + e^{(2)} \\ \implies & f = f^{(1)} + Unwrap(f_{res}^{(1)}) + e^{(2)} \\ \implies & f = f^{(1)} + f^{(2)} + e^{(2)} \\ \implies & f = \sum_{i=1}^{N} f^{(i)} + e^{(N)} \end{aligned}$$

Therefore, one can obtain successively better estimates by summing up the unwrapped estimates of each successive residual ($f_{res}^{(i)}$). This is highlighted by the last box in the flowchart depicted in Fig. 3.